DOI: 10.37190/ ABB-02247-2023-03

Fluid–structure interaction simulation for studying hemodynamics and rupture risk of patient-specific intracranial aneurysms

RUAN Chang[1], YU Qi[2], ZHOU Jingyuan[1], OU Xinying[1], LIU Yi[3*], CHEN Yu[1*]

1. Department of Applied Mechanics, Sichuan University（Chengdu 610065, Sichuan, China）

2. College of Mechanical Engineering, Sichuan University（Chengdu 610065, Sichuan, China）

3. Department of Neurosurgery, West China Hospital, Sichuan University（Chengdu 610041, Sichuan, China）

Corresponding Author: LIU Yi, Department of Neurosurgery, West China Hospital, Sichuan University（Chengdu 610041, Sichuan, China, liuyi@wchscu.cn; CHEN Yu, yu_chen@scu.edu.cn

Submitted: 9th May 2023

Accepted: 28th November 2023

Abstract

The role of regional hemodynamics in intracranial aneurysms (IAs) hemodynamics and rupture risk has been widely discussed based on numerical models over the past decades. The aim of this paper is to investigate hemodynamics and rupture risk with a complicated IA model. Fluid-structure interaction (FSI) simulations were performed to quantify the hemodynamic characteristics of the established IA models. Hemodynamic parameters, including wall shear stress (WSS), flow velocity, and flow pattern, were calculated and analyzed. In this paper, the risk assessment of intracranial aneurysms focuses on the mechanical properties of blood flow and blood vessel walls. Vortex flow and concentrated impact field during blood flow play a decisive role in the rupture and development of aneurysms. The uneven distribution of wall shear stress on the vessel wall has a great influence on growth and rupture. By observing the simulation results of rigid walls, risks can be predicted efficiently and accurately. This paper focuses on the relationship between hemodynamics and rupture risk with a double intracranial aneurysms disease mode and provides a new perspective on the treatment of intracranial aneurysms.

Keywords

intracranial aneurysms; fluid–structure interaction; hemodynamics; rupture risk; numerical simulation

Introduction

Currently, subarachnoid hemorrhage, mostly caused by intracranial aneurysm (IA) rupture, is accompanied by a high disability and mortality rate, and cerebrovascular disease has gradually become a major threat to human health. IAs are one of the fatal cerebrovascular pathologies, with 50%–60% mortality after rupture and a 30%–40% dependence rate among survivors(Amenta et al., 2012). More than 50% of IAs do not rupture in the individual's lifetime(Brisman, Song, & Newell, 2006). Therefore, to understand the rupture risk of IAs, understanding the different flow regimens in IAs is important(Saqr et al., 2020).

Aneurysm rupture may be related to aneurysm geometry, morphology, and complex flow activity. the main reason of the aneurism occurrence, growth and rupture can be explained by mechanical (hemodynamic) factors(Ivanov, Dol, Pavlova, & Aristambekova, 2014). To understand the blood flow dynamics of IAs, computational fluid dynamics (CFD) tools were adopted as an effective research tool to investigate numerous aspects of IA. Hemodynamics plays an important role in the natural history of IA, and low wall shear stress (WSS) was significantly associated with a higher risk of IA rupture(Tian et al., 2022). Important factors in predicting IA rupture are more complex flow, larger minimum WSS, and lower maximum low WSS area(W. Li et al., 2020). Meanwhile, deep learning is used to further realize the flow field prediction and avoid complex operations and the high computational cost of CFD(G. Li et al., 2021). Having high spatial resolution 4D flow magnetic resonance imaging is a feasible tool for assessing hemodynamics in IA(Medero, Ruedinger, Rutkowski, Johnson, & Roldán-Alzate, 2020). The fluid–structure interaction (FSI) presents a semi-realistic simulation environment to observe the structural interactions of blood and vessels, increasing the accuracy of the biomechanical study results(Rostam-Alilou, Jarrah, Zolfagharian, & Bodaghi, 2022). Fully coupled FSI simulations were performed to quantify the hemodynamic characteristics of IA models with various inflow angles, and the IA inflow angle was associated with the following hemodynamic changes(Mo, Meng, Yang, & Li, 2020).

FSI simulations were used to analyze a double IA disease mode in this study. We analyzed the variations of the hemodynamic characteristics to gain insights into the

relationship between hemodynamics and rupture risk with IA. Therefore, this study could be a useful reference for the rupture risk assessment of IAs.

Methods

In this paper, the hemodynamic research method of intracranial aneurysms is mainly based on numerical simulation. Based on medical image data, 3D digital modeling is carried out. The mechanical model is established by fluid mechanics and fluid-solid coupling theory, and the numerical results are obtained by simulation software.

Models

We present a case of a 67-year-old female patient from West China Hospital of Sichuan University. DSA (Distributed Systems Architecture) image examination showed two cystic protrusions near the anterior communicating artery, and she was diagnosed with an IA. The occurrence of two aneurysms in similar positions on the same blood vessel segment is extremely rare, and the more giant saccular aneurysm ruptured during the subsequent development of the aneurysm. Figure 1(a) shows the aneurysm examination results under imaging analysis.

Two image-processing software were needed to establish the vascular model. Mimics (Materialise's Interactive Medical Image Control System, MIMICS, Belgium) is a medical interactive image control system that can establish a 3D model for editing by inputting scanned data and outputting general CAD. It can also perform automatic unstructured meshwork for finite element calculations and is widely used in biomedical engineering, clinical research, and other fields. The imaging control system Mimics and medical modeling software 3-matic medical (Belgium, Materialise) were used to perform 3D reconstruction and smoothing of the Intracranial aneurysm and adjacent blood vessels. Figure 1(a) shows the processed 3D model.

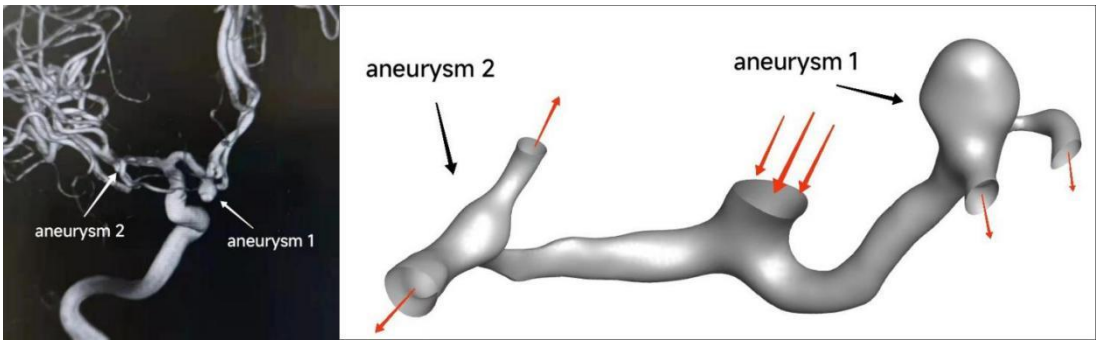

Fig 1(a) DSA data of aneurysm. (b) 3D reconstruction model

Cerebral artery wall thickness in different regions and the thickness of each area cannot be accurately measured using existing measurement techniques. The normal intracranial vascular thickness does not exceed 0.5 mm(Lee, Zhang, Takao, Murayama, & Qian, 2013). The mean wall thickness of IAs is 0.08–0.2 mm(Reorowicz et al., 2014). To simplify the calculation model, we adopted 0.1 mm for the modeling of the vascular wall.

The STL format model obtained by medical image reconstruction was imported into Rhino3D NURBS (Robert McNeel, USA) for shelling, and the solid model of the vascular wall was obtained by offsetting 0.1 mm outward and stored in STP format. Thus, the establishment of the digital vascular model was completed.

Mesh

The 3D digital model of blood vessels was divided into fluid and solid regions. The Fluent Meshing module in ANSYS and ANSYS Mechanical Enterprise module (Ansys, USA) were used to mesh the solid and fluid regions, respectively.

First, the flow field was meshed in Fluent Meshing, and the grid type was set to a polyhedral grid. The maximum and minimum mesh sizes were formed to 0.5 and 0.2 mm, respectively. The boundary layer was set to five layers, and the growth rate was 1.4. Because we focused on the study of stress-related values for the solid part, the tetrahedral grids were used to automatically divide the solid part because the solid region does not have high requirements for grids. The unit size was set to 0.2 mm. Figure 2 shows the numerical simulation model grid division. The number of fluid domain grids and nodes was 44,864 and 129,882, respectively. Moreover, the number of solid domain grids

and nodes was 51,870 and 104,105, respectively.

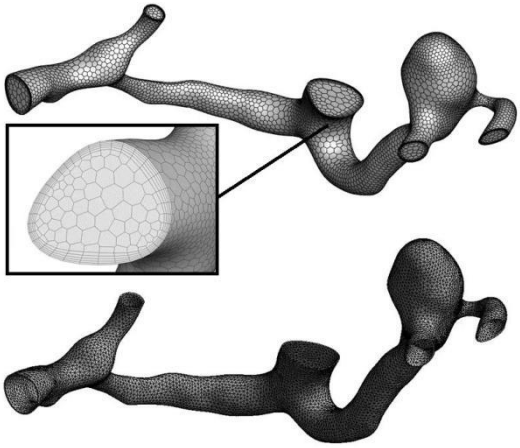

Fig 2 Fluid domain grid (upper). Solid domain grid (lower).

Mesh consideration

Mesh sensitivity study was conducted on the Fluid domain grid and the solid domain grid to offer a solution-independent element size. By only changing the maximum element size, several models with the same geometric parameters are obtained. The same boundary conditions are applied to this group of models for calculation and comparison. ~~Under the premise of changing the maximum unit size setting when the mesh is automatically divided, and ensuring that the geometric model and the remaining boundary conditions remain unchanged, the data calculated by several different models with different mesh numbers are calculated and compared.~~ The fluid part performs data results statistics on the steady-state maximum velocity and maximum WSS at different grid scales. Figure 3(a) shows the changes with the refinement of the grid. The maximum deformation curve of the solid part in one second is drawn for different grid scales. Figure 3(b) shows the change curve of different grid scales. The statistical results show that both the fluid grid and the solid grid have very good convergence. Further increase in the number of grids will not result in significant differences in results and may lead to an increase in computing resource consumption (such as simulation duration)(Oyejide, Awonusi, & Ige, 2023). Therefore, the mesh divided in the previous section is a suitable choice.

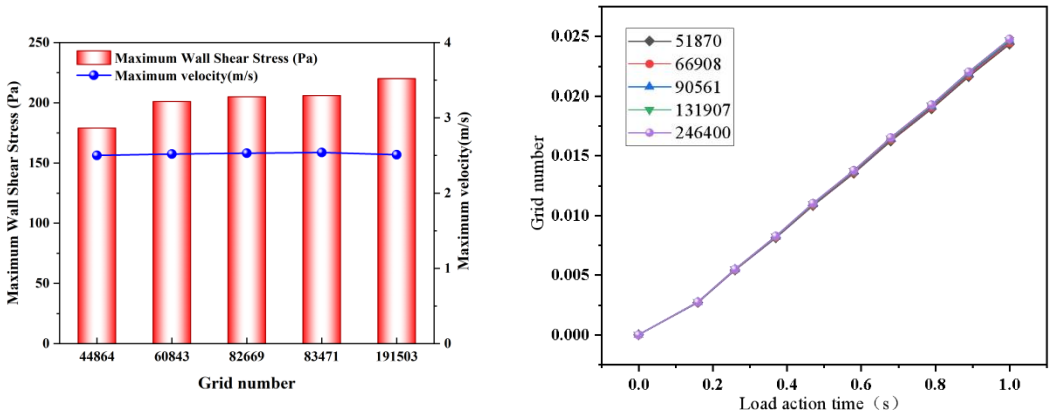

Fig3(a) Fluid domain grid sensitivity study. (b) Solid domain grid sensitivity study.

Fluid domain boundary conditions and governing equations

The blood flow in the blood vessels can be described using the Navier–Stokes and continuity equations. Based on relevant research, the use of Newtonian or non-Newtonian fluids does not make a substantial difference in hemodynamic calculations(J. R. Cebral et al., 2005). Therefore, we assumed that blood is a uniform, incompressible Newtonian fluid. Density and viscosity were set to $\rho = 1060\,kg/m^3$ and $\mu = 0.004Pa \cdot s$. Due to ~~Considering~~ the complexity of blood flow in the anterior communicating artery, this paper also considers the non-Newtonian effect of blood flow. The Carreau model is used to calculate the flow field of the blood flow as a non-Newtonian fluid to compare the difference between the two models in the calculation results. Time constant was set to $\lambda_{Ca} = 3.313s$, power-law index was set to $n = 0.3568$, zero shear viscosity and infinite shear viscosity were set to $\eta_0 = 0.056\,kg/m \cdot s$ and $\eta_0 = 0.0035\,kg/m \cdot s$ (Razavi, Shirani, & Sadeghi, 2011). The corresponding governing equations are as follows.

NS equation :

$$\rho\frac{\partial \vec{u}}{\partial x} + \rho(\vec{u}\cdot\nabla)\cdot\vec{u} + \nabla p - \mu\,\Delta\,\vec{u} = 0$$

Continuity equation :

$$\nabla\cdot\vec{u} = 0$$

$\vec{u}$——Blood flow velocity vector,m/s

p——Blood pressure,N/m^2

ρ——Blood density,kg/m^3

μ——Dynamic viscosity of blood,$Pa \cdot s$

The blood has both laminar flow and turbulence, which can be estimated using the Reynolds number (Re). The Reynolds number can be expressed as :

$$Re = \frac{\rho UL}{\mu}$$

Re——Reynolds number

U——Blood flow velocity in blood vessels,m/s

L——Blood vessel diameter,m

In the calculation, the inlet condition of the geometric model is the velocity inlet. In order to more effectively analyze the geometric effects of two different aneurysms on rupture, the steady-state inlet velocity is 0.37m/s(Qing, Wang, Fei, Liu, & Cao, 2009), the peak value of the blood flow velocity curve in the cardiac cycle (Fig 4)(Qiu, Fei, Zhang, & Cao, 2013). The geometric model exit condition was set to the pressure exit, the zero-pressure free flow boundary. In this study, the Reynolds number of the model was <201.4, so the laminar flow model was used.

But in fact, the flow in the cerebral arterial system is characterized by laminar to turbulent flow(Yi, Yang, Johnson, Bramlage, & Ludwig, 2022). Therefore, the shear stress transport (SST)$k-\omega$ turbulence model(Menter, 1994) is also used to calculate the flow field to compare the numerical differences brought by the two calculation methods. Equation to calculate turbulent viscosity, correlation coefficient and turbulent Reynolds number are as follow:

$$\mu_t = \alpha^* \frac{\rho k}{\omega}$$

$$\alpha^* = \frac{0.025 + \frac{Re_t}{6}}{1 + \frac{Re_t}{6}}$$

$$Re_t = \frac{\rho k}{\mu \omega}$$

μ_t——turbulent viscosity

ω——specific dissipation rate

Re_t——turbulent Reynolds number

Concurrently, the convergence residual of the fluid region was set to 10^{-7}.

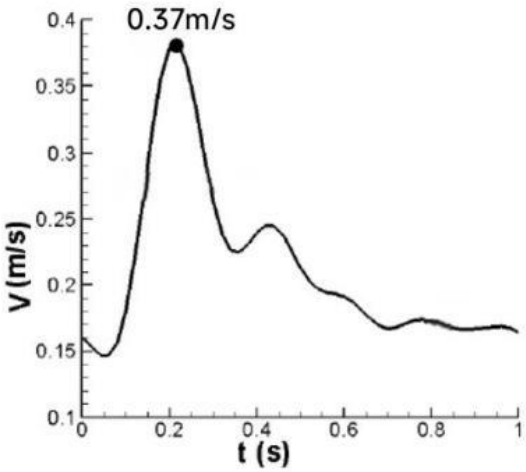

Fig 4 The curve of blood flow velocity in the inlet

Solid domain boundary conditions and governing equations

When the vessel wall is assumed to be isotropic linear elastic material, the elastic modulus and Poisson ratio of the blood vessel wall were $E = 5 \times 10^5 Pa$ and $\mu = 0.45$ (Reymond, Crosetto, Deparis, Quarteroni, & Stergiopulos, 2013). At the same time, when calculating the Von-Mises stress, the hyperelastic model was used to simulate the vessel wall in the ruptured aneurysm area. The Mooney-Rivlin two-parameter model of hyperelasticity was simulated in ANSYS to simulate the nonlinear elastic properties of the pipe wall. Select $c_{10} = 1.2879 \times 10^4 \mathrm{Pa}$, $c_{01} = 1.1578 \times 10^4 \mathrm{Pa}$, incompressibility coefficient $D = 0$ (Oliveira, Cardiff, Baccin, & Gasche, 2022). Additionally, the vascular wall thickness changes were ignored when the vascular wall dilates. The governing equation is the momentum conservation equation.

$$\rho_s a_s = \nabla \sigma_s$$

ρ_s——Solid density,kg/m^3

a_s——Local acceleration of solid region,m/s^2

σ_s——Solid stress tensor,N/m^2

The arterial outflow inlet adopts a fixed support boundary adjustment to simulate the motion constraints of the vascular segment in the body.

Fluid–solid interaction equations

Blood vessel wall is a compliant elastic material. The flow of blood through the blood vessels causes them to become deformed. Concurrently, blood vessel wall deformation will react with the blood and affect blood flow. The physical characteristics of the interface between blood and vessel wall conformed to the mechanical parts of fluid–solid coupling. In the calculation of the ground coupling problem in this paper, the calculation method of one-way coupling is adopted. The wall pressure obtained by calculating the flow field is transferred to the elastic wall in the form of boundary conditions as a load. At the interface, the following formula holds.

$$\sigma_s n_s = \sigma_f n_s$$

$$d_s = d_f$$

$$v_s = v_f$$

d——displacement, m

n——Wall normal vector

The subscripts *s* and f represent solid and fluid, respectively

Results

There are two main factors, WSS and flow velocity that are commonly used to analyze hemodynamic changes, and quantify most cardiovascular problems(Chaichana, Sun, & Jewkes, 2013). Blood flow exerts a force on the vessel wall and aneurysms and significantly influences WSS on the aneurysm wall. Therefore, studying the blood flow and pressure distribution in aneurysms and parent vessels is important(Isaksen et al., 2008).

Pressure

Figure 5 shows the pressure results of the wall and the inlet and outlet. From the pressure cloud diagram, it can be seen that when the blood flow is flowing, it will act on the blood vessel wall with uneven load. Therefore, the deformation of the blood vessel wall is also extremely complex, which also reveals the necessity of using the

fluid-structure interaction method for calculation. Comparing the pressure values on the inlet and outlet sections, it can be found that the aneurysm will significantly reduce the pressure at the outlet, so that the speed and direction of blood flow will also change.

However, whether pressure can be used as an influencing factor for rupture of intracranial aneurysms remains to be confirmed. Many studies have even reported that pressure is not an important hemodynamic factor in the rupture of intracranial aneurysms(Valencia, Morales, Rivera, Bravo, & Galvez, 2008). Therefore, this paper only regards pressure and pressure change as parameters in fluid-structure interaction calculation.

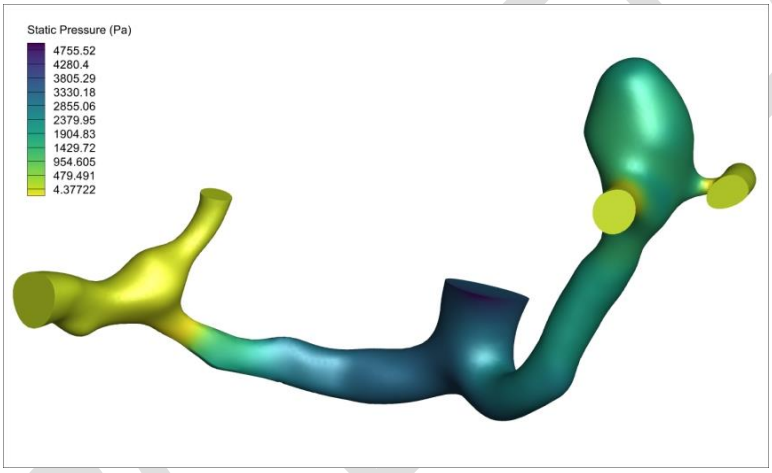

Fig5 Pressure distribution

Streamline

Figure 6(a) shows the final streamline analysis results under steady-state conditions. Because of the small diameter of the anterior communicating artery, the velocity of blood flow in the vessel increases considerably compared with inflow acceleration. Thus, blood flow is very complex because of this geometric scale mutation.

Blood flows at a higher rate in more giant aneurysms to create a vortex flow within the aneurysm, resulting in a constantly changing flow field within the aneurysm, making more physical properties unstable, such as the vessel inner wall being impacted by the more robust and changing direction of blood. Concurrently, the aneurysm continues to expand under the pressure of blood flow, ultimately leading to aneurysm rupture to a certain extent.

Due to the smaller inflow vessels in smaller aneurysms, the blood flow velocity in the narrow inflow vessel segment is remarkably high, resulting in a jet phenomenon. The generation of the jet also leads to energy loss; thus, the low blood flow velocity in another branch of the blood vessel. Concurrently, blood flow velocity near the vessel wall is not significantly affected due to the small cross-sectional area of the inflow vessel segment. Therefore, blood on the vessel wall surface does not have a more significant impact, resulting in a lower risk of aneurysm rupture in a short period.

Figure 6(b) shows the streamline obtained by using the (SST)$k-\omega$ turbulence model to calculate the flow field. Figure 6(c) shows the streamline obtained by using the Carreau model to calculate the flow field of the blood as a non-Newtonian fluid. The results of the blood flow velocity direction obtained by the three calculation methods are basically the same, and the position of the vortex formed is basically the same, and the maximum velocity has only a deviation of 1.3%. From the results, the simplification of the model studied in this paper using laminar flow model and Newtonian fluid will not cause deviations in the calculation results.

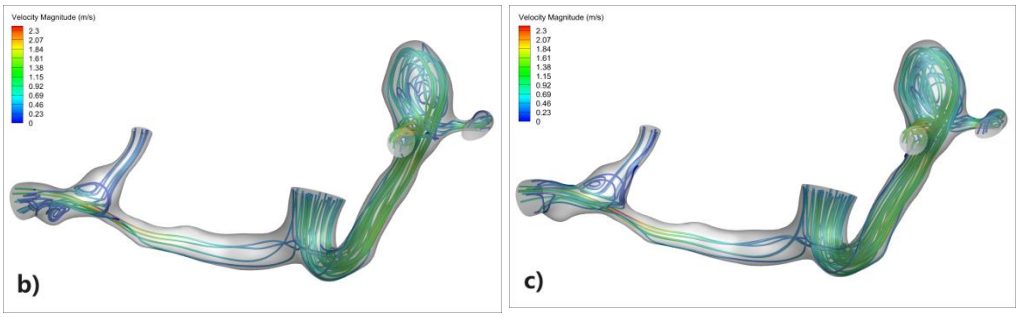

Fig 6 (a)Streamline of Newtonian fluid, laminar flow. (b) Streamline of Newtonian fluid, turbulence. (c) Streamline of Non-newtonian fluid, laminar flow.

WSS

WSS is the shear stress generated by the friction of viscous blood flow through the blood vessel wall. Figure 7(a) shows the WSS distribution. Figure 7(b) and (c) shows the WSS distribution on the border of subsequently ruptured and unruptured aneurysms, respectively. Because aneurysm lesions are affected by vascular geometry, they often have a remarkably high WSS(Philip, Bolem, Sudhir, & Patnaik, 2022). However, in the vicinity of the high WSS area, the lower region often has a large area, that is, the WSS gradient in the spatial distribution. In the subsequently ruptured aneurysms, the WSS near the neck is more extensive, and a large area of low WSS was found on the wall except at the top of the aneurysm. Concurrently, due to the relatively narrow vascular branches, there is a pronounced increase in WSS in the excessive area of tumor-bearing vessels and tumors. From the general distribution law, whether the aneurysm is smaller or giant, the maximum WSS is always at the transition between the aneurysm neck and blood vessel. In contrast, the WSS of the central part of the aneurysm is lower.

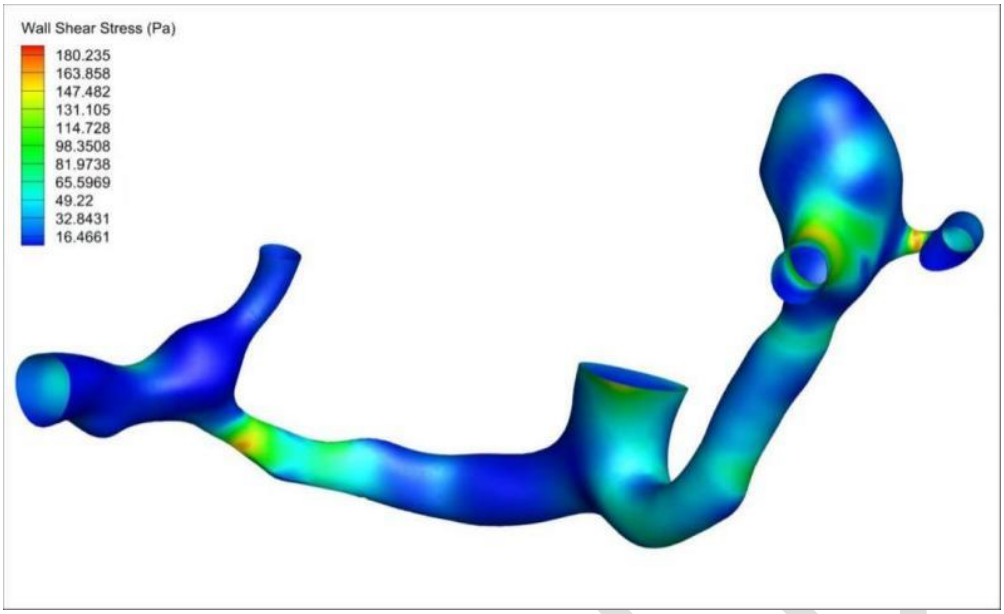

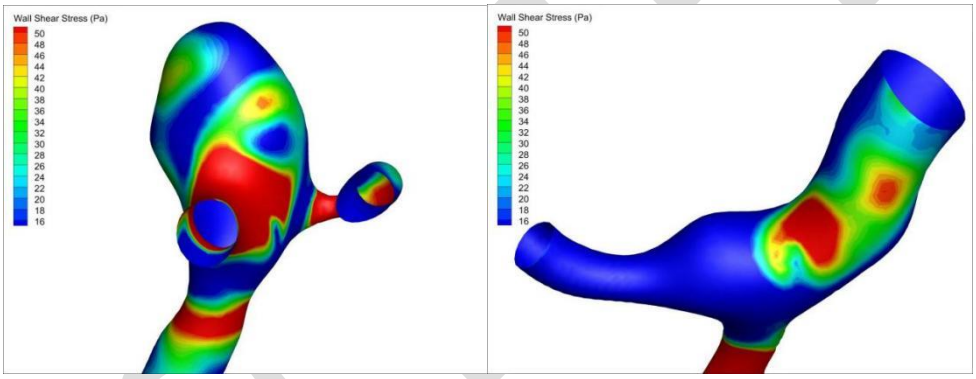

Fig7(a) WSS distribution map. (b) WSS distribution map of ruptured aneurysms. (c) WSS distribution map of unruptured aneurysms.

Von Mises

Based on the fourth material strength theory, the failure of elastic materials is generally due to the high Von Mises stress. If the vascular wall is considered a material, analysis of the Von Mises stress can estimate the possibility of rupture, and the maximum equivalent stress can predict the rupture point.

The equivalent stress distribution of the blood vessel is calculated using elastic material model and hyperelastic material models, respectively (Figure 8(a) and (b)). By observing the equivalent stress distribution, the Von Mises stress distribution at the aneurysm neck is high in the subsequently ruptured aneurysm, and its value is also significantly in the tumor part is higher than that in the smaller aneurysm. Therefore, Von

Mises pressure can be used as a reference standard for criticizing fracture risk.

By comparing the calculation results of the elastic and hyperelastic walls, Compared with the linear elastic model, the Von-Mises stress of the vascular wall with hyperelastic constitutive model is smaller in value, and the spatial distribution has a smaller gradient and a more uniform distribution. At the same time, the numerical results of the hyperelastic model also show that there is a significant stress enhancement at the neck of the aneurysm, which also explains a major reason for the rupture of the aneurysm. Although the location of the rupture predicted by the hyperelastic model and the linear elastic model is different, the results of the Von-Mises stress surge in the neck of the aneurysm are obtained. However, even if a relatively simple hyperelastic model is used, it is still prone to non-convergence in the calculation process, and the calculation time will be greatly increased, which is not suitable for clinical prediction and diagnosis.

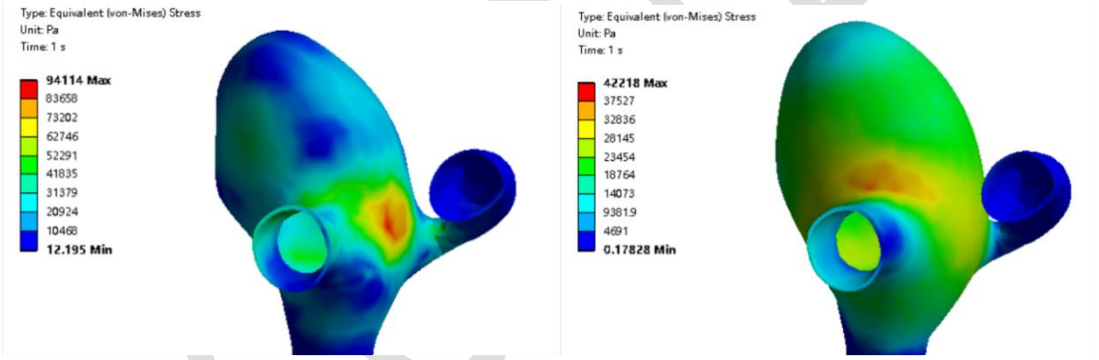

Fig 8(a) Von Mises stress distribution of the elastic model. (b) Von Mises stress distribution of the hyperelastic model.

Blood vessel deformation

Figure 9(a) shows the deformation results of the blood vessel wall by calculating the fluid–solid coupling of blood and blood vessel wall. Figure 9(b) and (c) shows the blood vessel shape before and after deformation, respectively. The parent vessel cannot easily deform if the aneurysm volume is small. For larger aneurysms, the maximum deformation does not occur at the dome but at the jet impingement point. Concurrently, the crown also has a large deformation. However, the deformation result is quite different from the actual situation because the tissue fluid in the physiological environment produces external pressure on the blood vessels. However, it can also provide a clinical reference for the

growth trend and treatment of IAs.

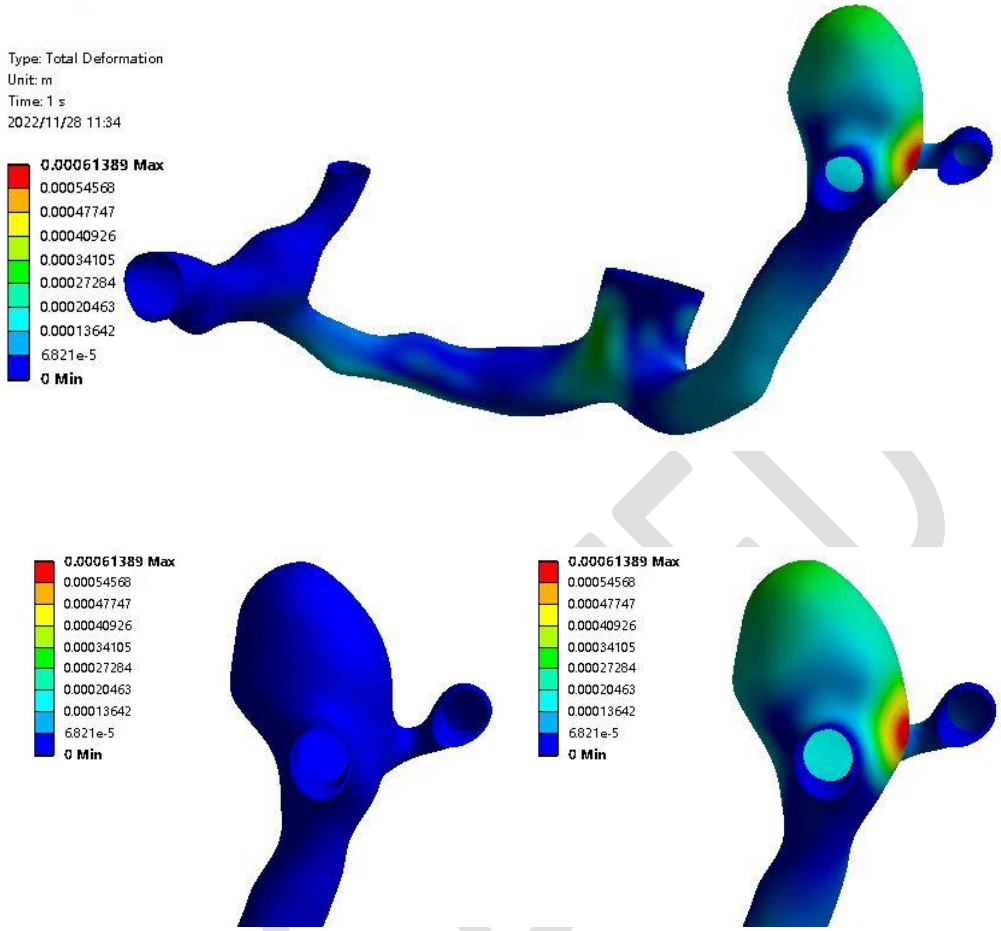

Fig 9(a) Vascular wall deformation. (b) Vascular configuration before deformation. (c) Vascular configuration after deformation.

Discussion

This study discussed selected cases with apparent characteristics. Two aneurysms were observed in a small range, and the larger aneurysm ruptured in the subsequent observation and treatment. Therefore, this case can screen many unrelated variables, such as genetic factors, patients' living habits, etc. Because the main blood flow affecting the two aneurysms was from the same inflow vessel, a certain degree of boundary condition simplification can be performed, and the branched small artery was considered the zero-pressure outlet boundary. In this study, the selected model and calculation method can intuitively explore the hemodynamic influencing factors of IA rupture. Factors affecting IA rupture are complex and result from a combination of blood flow and the

vessel wall. The most critical parameters in the hemodynamic study of IAs are blood flow velocity and WSS. Its dynamic effect is of great significance in assessing rupture risk.

In terms of blood flow velocity, vortex flow is present in more giant aneurysms and has a more significant rate. Some studies reported that vortex flow on the aneurysm wall causes significant damage and is the leading cause of aneurysm rupture(Hejčl et al., 2017). Pronounced vortex flow can be observed in subsequently ruptured aneurysms in the three-dimensional streamline diagram, whereas smaller aneurysms have no prominent vortex characteristics. Vortex intensity can be easily calculated and observed in hemodynamic parameters; thus, vortex size can be used as a critical evaluation criterion in the clinical prediction of rupture risk. Hoi et al. initially proposed the concept of shock domain(Hoi et al., 2004). which refers to the central area of the jet acting on the aneurysm wall. A significant difference can be found between the two aneurysms in the impact domain. When the inflow jet performs vertically on the vascular wall, the impact domain area takes the minimum value when other conditions are the same, and the velocity component in the average direction of the wall takes the maximum value. Aneurysms that subsequently ruptured had significantly smaller impact areas and were perpendicular to the wall at the neck, confirming that aneurysms with more incredible inflow velocity and smaller impact areas were more prone to rupture. Meanwhile, in the subsequent calculation results, the WSS values and equivalent stress in the impact region are significantly higher than those in other parts. Therefore, the jet effect of blood in blood vessels will have a more significant impact on the vessel wall. Because the speed of blood flow velocity in different physiological environments has different standards, intracranial blood flow velocity is difficult to determine physically. By comparing the blood flow characteristics of the two aneurysms, the vortex intensity and location of the impact region are prominent hemodynamic characteristics, which can be used as effective qualitative indicators. Aneurysms tend to have a higher rupture risk when significant vortex flow occurs in numerical simulations or when a concentrated area of blood flow impact can be observed(Fukazawa et al., 2015; Jiang et al., 2021). This predictive method can quickly assess the rupture risk clinically. Concurrently, in the design of interventional treatment programs, eddy currents must be eliminated, and concentrated blood flow shocks in

aneurysms should be reduced.

With regard to the most significant hemodynamic index in IAs, WSS is closely related to the morphology of aneurysms and parent vessels. The influence of aneurysm morphology can be intuitively investigated by studying WSS distribution(Valencia et al., 2008). Previous studies showed that remarkably high and low WSS could lead to aneurysm growth and rupture(Acevedo-Bolton et al., 2006; Juan R Cebral & Meng, 2012; Jou et al., 2005). Under the action of hemodynamics, smooth muscle cells of the aneurysm wall undergo two kinds of changes : (1) repair process of smooth muscle cells and collagen hyperplasia, (2) apoptosis of smooth muscle cells and other cells. When the two changes are in equilibrium, the aneurysm is stable, and the rupture risk is low. The subsequently ruptured aneurysms had high WSS areas, and the low WSS areas were unevenly distributed on the surface wall of the aneurysm. Aneurysm rupture may have resulted from high and low WSS. Studies of WSS distribution on the wall of anterior communicating artery aneurysms showed that the maximum WSS on the wall of ruptured aneurysms was often higher than that of unruptured aneurysms(Castro, Putman, Sheridan, & Cebral, 2009). Moreover, the maximum WSS was higher than that of the smaller aneurysm in the subsequently ruptured aneurysm. The highest WSS value can be used as the main factor to predict aneurysm rupture in smaller-diameter blood vessels and more complex blood flow environments. In the spatial WSS distribution, studies showed that the maximum WSS value on the aneurysm wall seems to be the aneurysm neck, and the minimum value is distributed at the top of the aneurysm. However, there is no obvious distribution(Shojima et al., 2005). Because WSS is the result of friction between blood and vessel walls, areas with complex geometries have high WSS. The WSS of the aneurysm neck or the vascular mutation area will be higher, whereas that of the central part of the cystic aneurysm will be lower. Comparative studies have also shown that the maximum effective stress in dome of larger aneurysms increases significantly and is more likely to rupture(Ivanov, Dol, & Polienko, 2016). Additionally, high WSS will induce IA formation and growth, but low WSS will lead to apoptosis, resulting in aneurysm wall degradation rupture(D'Arcangelo, Ambrosino, Giannuzzo, Gaetano, & Capogrossi, 2006; Liu, Fan, Xiang, Zhang, & Yang, 2016; Meng et al., 2007; Nixon, Gunel,

& Sumpio, 2010). Subsequent aneurysm rupture due to the large surface area results in a lower WSS area, and a large area of cell wall results in fracture. Due to the complexity of cerebral artery blood flow, there is no unified statement on the specific numerical criticism standard of WSS, and significant differences will be found under the influence of different simulation methods and prediction positions. Through the comparative analysis of the WSS values and spatial distribution of the two aneurysms, it can be estimated from the WSS spatial distribution gradient. Under complex geometric configurations, the WSS size changes significantly with the morphological characteristics of aneurysms, resulting in high and low WSS regions that are substantially different from typical vascular walls. A different spatial variation of WSS on the vessel and aneurysm walls may indicate that the aneurysm is morphologically a type with a high risk of rupture. The effect of excessively low WSS on the growth and rupture of aneurysms can indicate that WSS should be controlled at an expected range and occurrence of wall mutation area in the design of interventional therapy.

This study showed the fluid–solid coupling calculation of the hyperelastic wall and linear elastic wall, and the Von Mises stress distribution value on the wall was obtained. The calculation results of linear elastic and hyperelastic models show that the Von-Mises stress of the aneurysm neck is significantly enhanced, which has certain reference value for predicting the rupture of intracranial aneurysms. Even if different constitutive models have great differences in values, the distribution of the maximum Von-Mises stress can also be used to predict the possibility of future fracture. This view needs more cases to support. However, the hyperelastic model is far less than the linear elastic model in terms of calculation speed and convergence, so the linear elastic model is more practical for clinical analysis.

Limitations

This study has some limitations. First, the simulation process relies on several simplified assumptions. In order to obtain obvious comparative data, the simulation of blood flow cycle was not carried out, but the calculation simulation of steady state was

used to get the conclusion. And due to the convergence problem, the mechanical index of the whole model is not calculated when the hyperelastic model is used. The outlet boundary is simplified to a zero-pressure boundary in the calculation setting. Concurrently, this study only considers the inflow vessels that play a significant role in comparing the hemodynamic indexes of the two aneurysms under the same conditions and ensuring the convergence of calculation results. This study did not consider the complex blood flow in the anterior communicating artery. More accurate numerical results can be obtained if the above ideal assumptions are removed and the scheme closer to the actual situation is simulated. In addition, more hemodynamic parameters, such as oscillatory shear index, pressure difference, etc., should be considered in the calculation results to better explore the influencing factors of rupture and draw a more comprehensive conclusion(Murayama, Fujimura, Suzuki, & Takao, 2019). Therefore, the conclusions verified in this study need more forward-looking research for further improvement.

Conclusions

This article aimed to find the dominant hemodynamic factors leading to the growth and rupture of IAs through a particular case of IAs. Through CDF-based hemodynamic simulation, significant differences were found between ruptured and unruptured aneurysms in blood flow, WSS numerical distribution, and vascular deformation. Parameters, such as eddy current, impact domain, high and low WSS distribution, equivalent stress, and deformation degree, will mostly lead to aneurysm rupture.

Concurrently, by comparing the equivalent stress calculation results of hyperelastic material walls and elastic material walls, the fracture point should be predicted more accurately by fluid–solid coupling simulation, which is the most accurate simulation method and of great significance to clinical research. However, by comparing numerical results, the data calculated by fluid-structure coupling with linear elastic wall also have the ability to predict the fracture point. Through the processing method in this paper, the risk assessment of the rupture point of intracranial aneurysms can be carried out in an hour after the medical imaging data is obtained. It can provide auxiliary guidance for the

treatment plan with minimal cost.

Ethic statement：

This study was approved by the Ethics Committee of West China Hospital of Sichuan University (No. KS2019093). All patients gave their written informed consent.

Conflicts of Interest:

None

Funding:

This study was funded by 1·3·5 project for disciplines of excellence–Clinical Research Incubation Project, West China Hospital, Sichuan University (No. 2018HXFH007).

Ethical Approval:

Not required

References

Acevedo-Bolton, G., Jou, L.-D., Dispensa, B. P., Lawton, M. T., Higashida, R. T., Martin, A. J., . . . Saloner, D. (2006). Estimating the hemodynamic impact of interventional treatments of aneurysms: numerical simulation with experimental validation: technical case report. *Neurosurgery, 59*(2), E429-E430.

Amenta, P. S., Yadla, S., Campbell, P. G., Maltenfort, M. G., Dey, S., Ghosh, S., . . . Gonzalez, L. F. (2012). Analysis of nonmodifiable risk factors for intracranial aneurysm rupture in a large, retrospective cohort. *Neurosurgery, 70*(3), 693-701.

Brisman, J. L., Song, J. K., & Newell, D. W. (2006). Cerebral aneurysms. *New England journal of medicine, 355*(9), 928-939.

Castro, M. A., Putman, C. M., Sheridan, M. J., & Cebral, J. R. (2009). Hemodynamic Patterns of Anterior Communicating Artery Aneurysms: A Possible Association with Rupture. *American Journal of Neuroradiology, 30*(2), 297. doi:10.3174/ajnr.A1323

Cebral, J. R., Castro, M. A., Appanaboyina, S., Putman, C. M., Millan, D., & Frangi, A. F. (2005). Efficient pipeline for image-based patient-specific analysis of cerebral aneurysm hemodynamics: technique and sensitivity. *IEEE Transactions on Medical Imaging, 24*(4), 457-467. doi:10.1109/TMI.2005.844159

Cebral, J. R., & Meng, H. (2012). Counterpoint: realizing the clinical utility of computational fluid dynamics—closing the gap. In (Vol. 33, pp. 396-398): Am Soc Neuroradiology.

Chaichana, T., Sun, Z., & Jewkes, J. (2013). Hemodynamic impacts of left coronary stenosis: A patient-specific analysis. *Acta of Bioengineering and Biomechanics, 15*(3).

D'Arcangelo, D., Ambrosino, V., Giannuzzo, M., Gaetano, C., & Capogrossi, M. C. (2006). Axl receptor activation mediates laminar shear stress anti-apoptotic effects in human endothelial cells. *Cardiovascular research, 71*(4), 754-763.

Fukazawa, K., Ishida, F., Umeda, Y., Miura, Y., Shimosaka, S., Matsushima, S., . . . Suzuki, H. (2015). Using computational fluid dynamics analysis to characterize local hemodynamic features of middle cerebral artery aneurysm rupture points. *World neurosurgery, 83*(1), 80-86.

Hejčl, A., Švihlová, H., Sejkorová, A., Radovnický, T., Adámek, D., Hron, J., . . . Sameš, M. (2017). Computational fluid dynamics of a fatal ruptured anterior communicating artery aneurysm. *Journal of Neurological Surgery Part A: Central European Neurosurgery, 78*(06), 610-616.

Hoi, Y., Meng, H., Woodward, S. H., Bendok, B. R., Hanel, R. A., Guterman, L. R., & Hopkins, L. N. (2004). Effects of arterial geometry on aneurysm growth: three-dimensional computational fluid dynamics study. *Journal of Neurosurgery, 101*(4), 676-681. doi:10.3171/jns.2004.101.4.0676

Isaksen, J. G., Bazilevs, Y., Kvamsdal, T., Zhang, Y., Kaspersen, J. H., Waterloo, K., . . . Ingebrigtsen, T. (2008). Determination of Wall Tension in Cerebral Artery Aneurysms by Numerical Simulation. *Stroke, 39*(12), 3172-3178. doi:10.1161/STROKEAHA.107.503698

Ivanov, D., Dol, A., Pavlova, O., & Aristambekova, A. (2014). Modeling of human circle of Willis with and without aneurisms. *Acta of Bioengineering and Biomechanics, 16*(2), 121-129.

Ivanov, D., Dol, A., & Polienko, A. (2016). Patient-specific hemodynamics and stress-strain state of cerebral aneurysms. *Acta of Bioengineering and Biomechanics, 18*(2), 9--17.

Jiang, Y., Lu, G., Ge, L., Huang, L., Wan, H., Wan, J., & Zhang, X. (2021). Rupture point hemodynamics of intracranial aneurysms: case report and literature review. *Annals of Vascular Surgery-Brief Reports and Innovations, 1*(2), 100022.

Jou, L.-D., Wong, G., Dispensa, B., Lawton, M. T., Higashida, R. T., Young, W. L., & Saloner, D. (2005). Correlation between lumenal geometry changes and hemodynamics in fusiform intracranial aneurysms. *American Journal of Neuroradiology, 26*(9), 2357-2363.

Lee, C. J., Zhang, Y., Takao, H., Murayama, Y., & Qian, Y. (2013). The influence of elastic upstream artery length on fluid–structure interaction modeling: A comparative study using patient-specific cerebral aneurysm. *Medical Engineering & Physics, 35*(9), 1377-1384. doi:https://doi.org/10.1016/j.medengphy.2013.03.009

Li, G., Song, X., Wang, H., Liu, S., Ji, J., Guo, Y., . . . Wang, X. (2021). Prediction of cerebral aneurysm hemodynamics with porous-Medium models of flow-diverting stents via deep learning. *Frontiers in Physiology, 12*, 733444.

Li, W., Wang, S., Tian, Z., Zhu, W., Zhang, Y., Zhang, Y., . . . Liu, J. (2020). Discrimination of intracranial aneurysm rupture status: patient-specific inflow boundary may not be a must-have condition in hemodynamic simulations. *Neuroradiology, 62*, 1485-1495.

Liu, J., Fan, J., Xiang, J., Zhang, Y., & Yang, X. (2016). Hemodynamic characteristics of large unruptured internal carotid artery aneurysms prior to rupture: a case control study. *Journal of NeuroInterventional Surgery, 8*(4), 367-372.

Medero, R., Ruedinger, K., Rutkowski, D., Johnson, K., & Roldán-Alzate, A. (2020). In vitro assessment of flow variability in an intracranial aneurysm model using 4D flow MRI and tomographic PIV. *Annals of biomedical engineering, 48*, 2484-2493.

Meng, H., Wang, Z., Hoi, Y., Gao, L., Metaxa, E., Swartz, D. D., & Kolega, J. (2007). Complex hemodynamics at the apex of an arterial bifurcation induces vascular remodeling resembling cerebral aneurysm initiation. *Stroke, 38*(6), 1924-1931.

Menter, F. R. (1994). Two-equation eddy-viscosity turbulence models for engineering applications. *AIAA journal, 32*(8), 1598-1605.

Mo, X., Meng, Q., Yang, X., & Li, H. (2020). The impact of inflow angle on aneurysm hemodynamics: a simulation study based on patient-specific intracranial aneurysm models. *Frontiers in Neurology, 11*, 534096.

Murayama, Y., Fujimura, S., Suzuki, T., & Takao, H. (2019). Computational fluid dynamics as a risk assessment tool for aneurysm rupture. *Neurosurgical focus, 47*(1), E12.

Nixon, A. M., Gunel, M., & Sumpio, B. E. (2010). The critical role of hemodynamics in the development of cerebral vascular disease: a review. *Journal of Neurosurgery, 112*(6), 1240-1253.

Oliveira, I. L., Cardiff, P., Baccin, C. E., & Gasche, J. L. (2022). A numerical investigation of the mechanics of intracranial aneurysms walls: Assessing the influence of tissue hyperelastic laws and heterogeneous properties on the stress and stretch fields. *Journal of the Mechanical Behavior of Biomedical Materials, 136*, 105498. doi:https://doi.org/10.1016/j.jmbbm.2022.105498

Oyejide, A. J., Awonusi, A. A., & Ige, E. O. (2023). Fluid-structure interaction study of hemodynamics and its biomechanical influence on carotid artery atherosclerotic plaque deposits. *Medical Engineering & Physics, 117*, 103998. doi:https://doi.org/10.1016/j.medengphy.2023.103998

Philip, N. T., Bolem, S., Sudhir, B. J., & Patnaik, B. S. V. (2022). Hemodynamics and bio-mechanics of morphologically distinct saccular intracranial aneurysms at bifurcations: Idealised vs Patient-specific geometries. *Computer Methods and Programs in Biomedicine, 227*, 107237. doi:https://doi.org/10.1016/j.cmpb.2022.107237

Qing, W., Wang, W.-z., Fei, Z.-m., Liu, Y.-z., & Cao, Z.-m. (2009). Simulation of blood flow in intracranial ICA-pcoma aneurysm via computational fluid dymamics modeling. *Journal of Hydrodynamics, Ser. B, 21*(5), 583-590.

Qiu, X.-n., Fei, Z.-m., Zhang, J., & Cao, Z.-m. (2013). Influence of high-porosity mesh stent on hemodynamics of intracranial aneurysm: A computational study. *Journal of Hydrodynamics, 25*(6), 848-855.

Razavi, A., Shirani, E., & Sadeghi, M. (2011). Numerical simulation of blood pulsatile flow in a stenosed carotid artery using different rheological models. *Journal of Biomechanics, 44*(11), 2021-2030.

Reorowicz, P., Obidowski, D., Klosinski, P., Szubert, W., Stefanczyk, L., & Jozwik, K. (2014). Numerical simulations of the blood flow in the patient-specific arterial cerebral circle region. *Journal of Biomechanics, 47*(7), 1642-1651. doi:https://doi.org/10.1016/j.jbiomech.2014.02.039

Reymond, P., Crosetto, P., Deparis, S., Quarteroni, A., & Stergiopulos, N. (2013). Physiological

simulation of blood flow in the aorta: Comparison of hemodynamic indices as predicted by 3-D FSI, 3-D rigid wall and 1-D models. *Medical Engineering & Physics, 35*(6), 784-791. doi:https://doi.org/10.1016/j.medengphy.2012.08.009

Rostam-Alilou, A. A., Jarrah, H. R., Zolfagharian, A., & Bodaghi, M. (2022). Fluid–structure interaction (FSI) simulation for studying the impact of atherosclerosis on hemodynamics, arterial tissue remodeling, and initiation risk of intracranial aneurysms. *Biomechanics and modeling in mechanobiology, 21*(5), 1393-1406.

Saqr, K. M., Rashad, S., Tupin, S., Niizuma, K., Hassan, T., Tominaga, T., & Ohta, M. (2020). What does computational fluid dynamics tell us about intracranial aneurysms? A meta-analysis and critical review. *Journal of Cerebral Blood Flow & Metabolism, 40*(5), 1021-1039.

Shojima, M., Oshima, M., Takagi, K., Torii, R., Nagata, K., Shirouzu, I., . . . Kirino, T. (2005). Role of the bloodstream impacting force and the local pressure elevation in the rupture of cerebral aneurysms. *Stroke, 36*(9), 1933-1938.

Tian, Z., Li, X., Wang, C., Feng, X., Sun, K., Tu, Y., . . . Duan, C. (2022). Association Between Aneurysmal Hemodynamics and Rupture Risk of Unruptured Intracranial Aneurysms. *Frontiers in Neurology, 13*.

Valencia, A., Morales, H., Rivera, R., Bravo, E., & Galvez, M. (2008). Blood flow dynamics in patient-specific cerebral aneurysm models: the relationship between wall shear stress and aneurysm area index. *Medical Engineering & Physics, 30*(3), 329-340.

Yi, H., Yang, Z., Johnson, M., Bramlage, L., & Ludwig, B. (2022). Developing an in vitro validated 3D in silico internal carotid artery sidewall aneurysm model. *Frontiers in Physiology, 13*, 1024590.